ZnO Particulate Matter Requires Cell Contact for Toxicity in Human Colon Cancer Cells

Philip J. Moos,* Kevin Chung, David Woessner, Matthew Honeggar, N. Shane Cutler, and John M. Veranth

Department of Pharmacology and Toxicology, University of Utah, L. S. Skaggs Pharmacy, Room 201, 30 S 2000 East, Salt Lake City, Utah 84112

Received June 18, 2009

There is ongoing concern regarding the toxicity of nanoparticles with sizes less than 100 nm as compared to larger particles of the same nominal substance. Two commercial ZnO types, one sold as a 8−10 nm powder and the other described as −325 mesh (<44 μm) powder, were evaluated in human colon-derived RKO cells. The powders had a volume-to-surface area ratio equivalent to 40 and 330 nm spheres, respectively. Both materials formed micrometer-sized agglomerates in cell culture media. The nanosized ZnO was more cytotoxic than the micrometer-sized ZnO with LC_{50} values of 15 ± 1 and 29 ± 4 $\mu g/cm^2$, respectively. Transfer of Zn from the solid phase to the cell culture media in the presence of RKO cells was time- and concentration-dependent. However, direct particle−cell contact was required for RKO cell cytotoxicity, and the toxicity of particles was independent of the amount of soluble Zn in the cell culture media. The mechanism of cell death includes the disruption of mitochondrial function. Robust markers of apoptosis, Annexin V staining, loss of mitochondrial potential, and increased generation of superoxide were observed when cells were treated with ZnO particulate matter but not when treated with comparable concentration of a soluble Zn salt. Both ZnO samples induced similar mechanisms of toxicity, but there was a statistically significant increase in potency per unit mass with the smaller particles.

Introduction

Manufactured nanoparticles are being marketed as having unique properties due to their size, shape, surface area, and composition as compared to bulk material, but there remain concerns regarding toxicities associated with these novel materials (*1*−*3*). This is especially relevant for oxides of Fe, Si, Ti, and Zn as these compounds are used in foods, cosmetics, and other consumer products (*4, 5*). Accidental exposure to nanosized zinc oxide from children accidentally eating sunscreen products is a typical public concern, motivating the study of the effects of nanomaterials in the colon (*3, 6*). In our previous work, immortalized human cells were used to study biochemical responses to several pairs of micrometer- and nanosized metal and ceramic oxide particles to test for size-dependent effects (*7*). ZnO appeared to induce cell responses at lower exposure concentrations that the other tested oxides. Toxicity from ZnO nanoparticles has been reported in a broad range of biological systems (*8*−*15*), but the mechanisms are not well understood. In humans, high doses of ZnO can induce metal fume fever, which is characterized by pulmonary toxicity (*16*−*20*). The toxicity to other organ systems is less clear, but Zn can irritate the gastrointestinal tract, can induce emesis, and can be associated with an impaired inflammatory response (*21, 22*). Zinc toxicity in certain organisms is due to the dissolution of Zn ions (*9*). ZnO is considered nearly insoluble in water, but solubility increases in acid environments and in the presence of chelators. In a murine model, the development of ZnO tolerance appears to enlist genes like metallothionein (*23*) that sequester Zn^{2+}.

This study tested the in vitro response of human colon-derived RKO cells to two types of ZnO powders, one of which was marketed as a nanomaterial and the other described by mechanical screen size. These chemical reagents are representative of commercially available powders that are sold in bulk quantity as manufacturing ingredients. We tested these two materials to evaluate their relative cytotoxicity and to determine if they have common mechanisms of toxicity. One important aim of this study was to determine if the ZnO toxicity in a human colon cell line was dependent on Zn^{2+} ion liberation from ZnO or direct ZnO contact. We show that ZnO particles liberate Zn^{2+}, but the levels of Zn released are insufficient to promote mitochondrial dysfunction and cell death unless the particulate is in contact with the cells.

Experimental Procedures

Materials. Advanced DMEM, Glutamax, MitoProbe JC-1 Assay Kit, Vybrant Apoptotic Assay Kit #2, MitoSOX Red, and Hank's balanced salt solution with Ca and Mg (HBSS) were purchased from Invitrogen (Carlsbad, CA). Fetal bovine serum was purchased from Hyclone (Logan, UT). The RKO cell line was purchased from American Tissue Type Culture Collection (Manassas, VA). Cell Counting Kit-8 (CCK-8) was purchased from Dojindo (Gaithersburg, MD). Transwells with 0.4 μm polyester membranes (product number 3450) were purchased from Corning (Corning, NY), and Slide-A-Lyzer 10 kDa cassettes (product number 66383) were purchased from Pierce (Rockford, IL). ZnO particulate matter was purchased from Alpha Aesar (Ward Hill, MA). The catalog number 44299 ZnO is marketed as an 8−10 nm aerodynamic particle size powder, while the catalog number 11558 material is identified as being −325 mesh (approximately 44 μm screen opening) powder. These source materials will be referred to as nZnO and mZnO, respectively, where n = designates "nano" and m = designates "micro", even though the mZnO actually has significant content of submicrometer particles, as discussed below.

Cell Culture. RKO colon cancer cells were used as a representative colon cell line and were maintained in Advanced DMEM

* To whom correspondence should be addressed. Tel: 801-585-5952. Fax: 801-585-5111. E-mail: philip.moos@utah.edu.

10.1021/tx900203v
Published on Web 02/15/2010

supplemented with 1% Glutamax and 2% fetal bovine serum. For experiments that used particulate matter, the nanomaterial was sterilized using 70% EtOH and vacuum-dried, then added to medium, and sonicated for 15 min in a Cole-Parmer 8890 water bath sonicator to resuspend the particulate matter.

Zinc Analysis. Inductively coupled plasma (ICP) spectrometry (Perkin-Elmer Optima 3100 XL) was used to determine the Zn content in cell culture media following addition of ZnO particulate matter. The instrument was calibrated using SPEX CertiPrep Laboratory Performance Check Standard 1 (Metuchen, NJ). Experimental samples were prepared by collecting media in microfuge tubes and centrifuged at 20000*g* for 30 min to remove any ZnO particles. An aliquot was carefully removed from the top of the microfuge tube to avoid disrupting any pellet, and a 600 μL sample was evaluated by ICP. The results were collected in ppm using WinLab32 for ICP software (v. 3.4.0.0253).

Particle Size. The particle size and shape were verified by transmission and scanning electron microscopy. Samples of the ZnO powders for TEM were suspended at approximately 0.1 mg/mL in water containing 1% of FL-70 surfactant (Fisher Scientific), vortexed, and then dispersed by the same sonication used for the cell treatments. Approximately 1 μL of the suspension was placed on a carbon grid, air-dried, and examined on a Tecnai G2 transmission electron microscope at 120 kV. Samples for SEM were prepared by dispersal of dry powder on conducting carbon tape. The particle surface area per mass was measured by nitrogen adsorption (BET single point method) using a Quantachrome Monosorb analyzer. The volume−surface mean diameter, defined as the diameter of uniform spheres that have the same ratio of volume to surface area as the powder mixture, was calculated from the specific surface area measurement assuming spherical particles using eq 1 with a ZnO density of 5.6 g/cm^3.

$$d_{sm} = \frac{6}{\rho \times SA_{BET}} \quad (1)$$

where d_{sm} is the volume−surface mean diameter, ρ is the solid density, and SA_{BET} is the specific surface area measured by gas adsorption. This equation is derived from the geometric relationship for a sphere:

$$\frac{\text{surface}}{\text{mass}} = \frac{\pi d^2}{\rho \frac{\pi}{6} d^3} \quad (2)$$

The size distribution of the ZnO particle agglomerates was measured by dynamic light scattering (DLS) using a Malvern Zetasizer Nano ZS. Measurements were made immediately after sonication and after overnight incubation using particle suspensions in cell culture media using the same handling and dispersal as used for the RKO cell treatments.

Viability Assays. Cellular viability was determined using Cell Counting Kit-8 (CCK-8), which relies on tetrazolium salt reduction by NADH in viable cells (*24*). Briefly, cells were seeded into 48 well plates at 2−4 × 10^4 cells/well and allowed to recover overnight. Nanoparticles were evaluated at concentrations ranging from 1−100 μg/cm^2. The cell cultures were incubated with the particulate matter for 24 h and then assessed for viability. Following the treatment period, medium was aspirated and replaced with 4% CCK-8 in cell culture medium. Absorbance at 460 and 650 nm was measured after incubation at 37 °C until the reagent developed sufficiently for maximal reading using a Perkin-Elmer VictorV^3 Multimode Microplate Reader. Cell-free samples were run to rule out any interaction between the nanoparticles and the colormetric reagent.

Another, more sensitive measure of viability that we utilized was propidium iodide (PI) exclusion. Cells were seeded into six-well plates at a density of ∼2 × 10^5 cells/well and were allowed to grow overnight. The culture medium was refreshed at the time of treatment. Cells were trypsinized, washed, and resuspended in 1 mL of HBSS to which 2 μL of 100 μg/mL PI was added prior to cytometric analysis. Cellular fluorescence was determined 24 h after treatment using a Cell Lab Quanta SC flow cytometer (Beckman Coulter). For each assay, a minimum of 10000 events per sample was recorded.

Apoptotic Assays. Three cytometric assays were used to evaluate markers of apoptosis and mitochondrial status using a CellLab Quanta SC flow cytometer.

Annexin V/PI Staining. The Vybrant Apoptotic Assay Kit #2 was used in a dual color cytometric assay to evaluate Annexin V as an early marker of cell death along with PI exclusion using a CellLab Quanta SC flow cytometer. Cells were trypsinized, washed, and resuspended in 100 μL of annexin-binding buffer, 5 μL of Alexa-488 conjugated Annexin V, and 1 μL of 100 μg/mL PI was for a 15 min incubation, and then, the cells were diluted to 500 μL prior to cytometric evaluation. Cellular fluorescence was determined following 24 h after treatment with ZnO, and a minimum of 10000 events per sample was recorded. The events were classified as follows: Cells that were not stained represented viable cells, Annexin V positive represented early apoptotic cells, and Annexin V plus PI double positive represented late apoptotic or necrotic cells.

Mitochondrial Potential. The MitoProbe JC-1 Assay Kit was used to measure the mitochondrial potential; 1 μM JC-1 was added to medium of cells attached to six-well plates after ZnO particulate treatment. Cells were incubated at 37 °C with 5% CO_2 and 95% air for 30 min and then trypsinized, washed, and resuspended in HBSS. JC-1 fluorescence at 525 (JC-1 "green") and 575 nm (JC-1 "red" or "J aggregates") was determined for each sample. JC-1 fluoresces green when the mitochondrial potential has been depolarized and forms aggregates that fluoresce red when the mitochondrion is polarized (*25*). Carbonyl cyanide 3-chlorophenylhydrazone (CCCP), 25 μM, was used as a positive control to disrupt the mitochondrial membrane potential. Cellular fluorescence was determined 24 h after treatment by flow cytometry, and for each sample, a minimum of 10000 events per sample was recorded.

MitoSOX Assay. Measurement of superoxide production was performed with MitoSOX Red. Cells were treated with ZnO particulate matter or $ZnCl_2$, trypsinized, washed, resuspended in 1 mL of HBSS, and then incubated with 5 μM MitoSOX Red for 10 min. Cellular fluorescence was determined 24 h after the Zn treatment by flow cytometry, a minimum of 10000 events per sample was measured, and the percent of the population that displayed MitoSOX fluorescence was recorded.

Statistical Analysis. One-way ANOVA was used to determine statistical significance among samples (GraphPad InStat Version 3.06). Bonferroni multiple comparisons posthoc testing was used to establish significance among the treatment groups with $p < 0.05$ considered significant.

Results

The nZnO consisted of 20−60 nm irregular particles (Figure 1A), and the geometric size observed by TEM is consistent with the 45 nm volume−surface mean diameter calculated from the 24 m^2/g gas adsorption surface area measurement. These sizes are larger than the vendor's nominal 8−10 nm aerodynamic size. A loose aggregate has an aerodynamic diameter smaller than the physical cluster size, but conversion between geometric and aerodynamic size is imprecise for irregular particles. On the basis of our measurements, the nZnO was confirmed to consist of particles $d < 100$ nm and is therefore a nanomaterial by the common definition. The mZnO particles were very heterogeneous in shape and size, ranging from structures smaller than 100 nm to angular particles several micrometers in length as shown in the TEM (Figure 1B) and SEM (Figure 1C) images. The measured specific surface area was 3.2 m^2/g, which gives a calculated volume−surface mean diameter of 330 nm. Reconciling the size and morphology observed by electron microscopy with the high surface area measured by gas

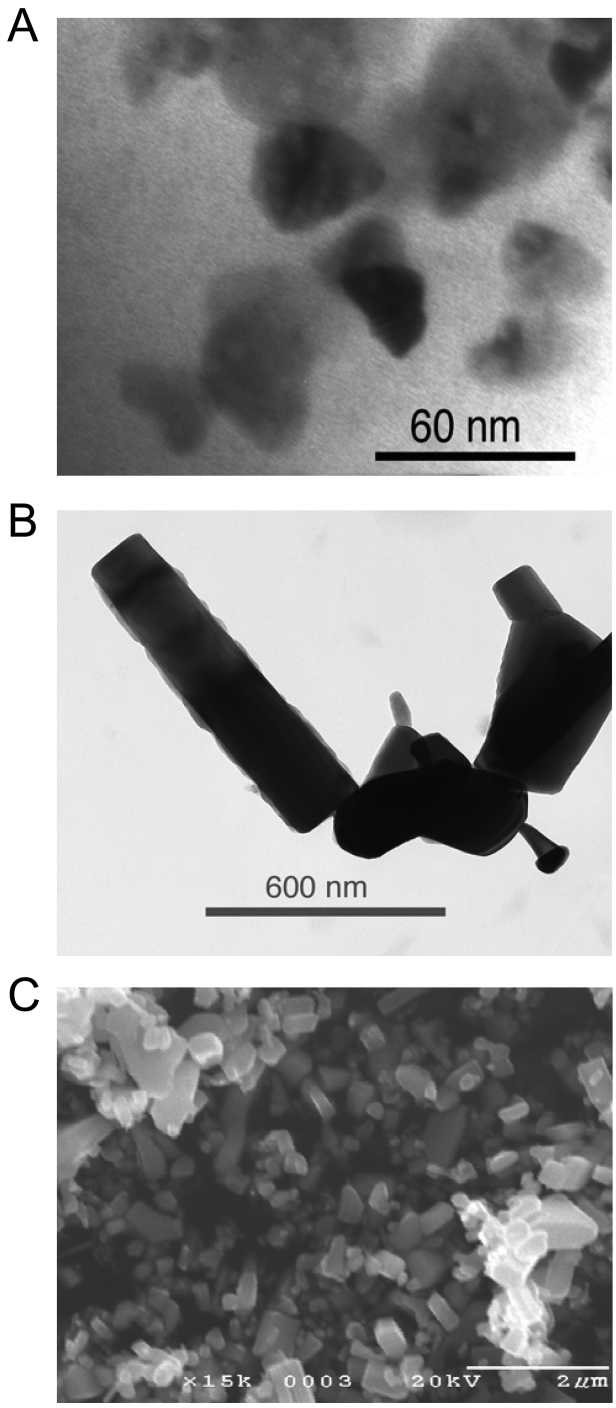

Figure 1. Electron microscopy of ZnO particulate matter. TEM images are (A) the nominal nanosized nZnO and (B) the nominal micrometer-sized mZnO powders. The SEM image (C) is also the mZnO. The images confirm that there is a size difference between the two products but that both are heterogeneous mixtures of particle sizes.

adsorption implies that the mZnO powder contains both fused aggregates of submicrometer particles and larger particles, with most of the mass in particles much smaller that the nominal 325 mesh cut size. Although the mZnO was sold as a conventional powder, it contains a significant amount of submicrometer particles. The nZnO and mZnO had a 7.5:1 ratio of specific surface area, so the two powders were still adequate to test the effect of particle size on biological responses. Measurement of particle size by DLS showed that in DMEM media with 2% serum both the nZnO and the mZnO formed agglomerates with a mode in the 500−2000 nm size range and a larger mode that was truncated by the instrument range. These

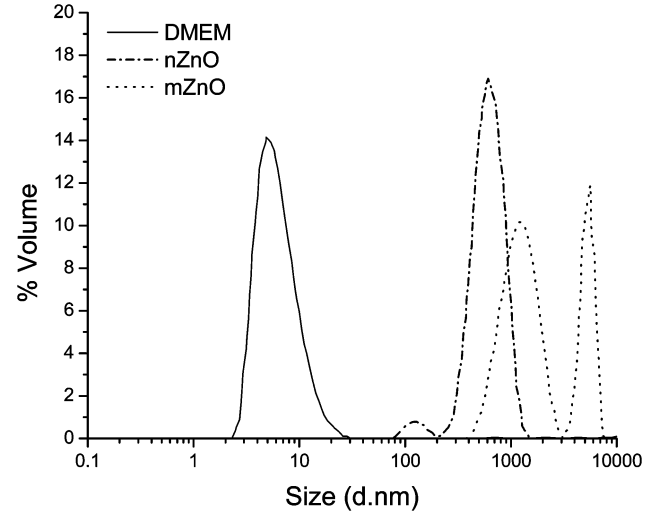

Figure 2. DLS evaluation of ZnO particles in cell culture media. Particle volume-scaled size distributions are shown for serum-containing DMEM media (solid line) and for nZnO (dash-dotted line) and mZnO (dotted line) in cell culture media immediately after sonication. Data are normalized by the instrument; therefore, peak heights cannot be compared between samples. This is a typical measurement, but exact size of the agglomerate modes varied with time, concentration, and handling.

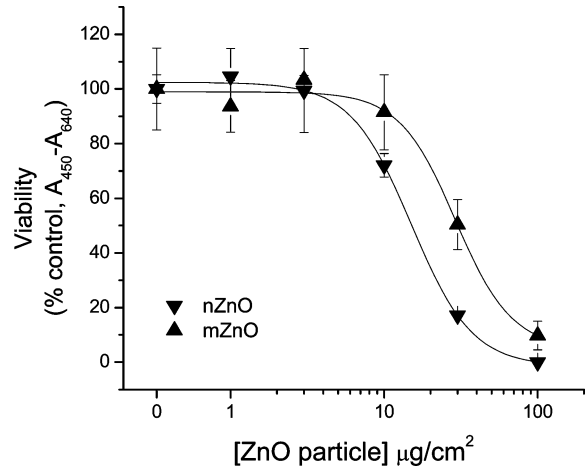

Figure 3. Cell viability following incubation with ZnO particulate matter. Cell viability was measured with a formazan-style assay following incubation with nano- (nZnO, ▼) and microsized (mZnO, ▲) ZnO particulate matter. The nZnO particulate was approximately twice as toxic as the mZnO particulate (LC_{50} concentrations of 15 ± 1 and 29 ± 4 $\mu g/cm^2$, respectively). The 10 ($p < 0.01$) and 30 $\mu g/cm^2$ ($p < 0.001$) concentrations displayed statistically significant differences in cell viability.

agglomerates were observed with 10 min of sonication (Figure 2) and after 24 h (data not shown). The exact size of the agglomerate mode varied with concentration and agitation, and the mode sizes should be regarded as a qualitative indication of the extent of aggregation due to the complex interaction between the cell culture media components and the particles. However, both visual observation of settling of the ZnO in the cell culture wells and the DLS data indicate that the cells were exposed to agglomerates much larger than 100 nm. The DLS results observed in this study are similar to the DLS results recently reported by others with silica particles (*26*).

We examined the in vitro toxicity of nZnO and mZnO (Figure 3). The nZnO was approximately twice as cytotoxic as the mZnO with LC_{50} concentrations of 15 ± 1 and 29 ± 4 $\mu g/cm^2$, respectively. There were statistically significant differences in viability between the nZnO- and the mZnO-treated cells for both

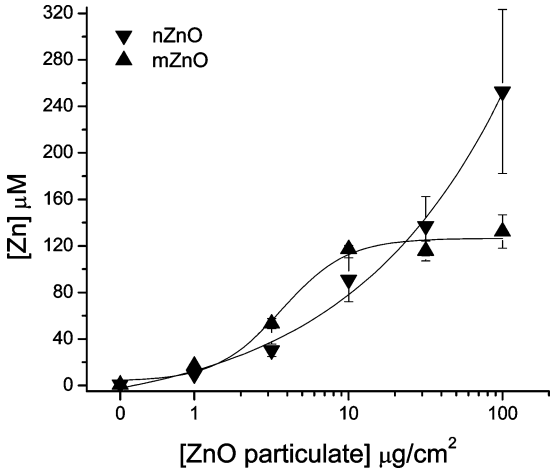

Figure 4. Soluble Zn concentrations measured by ICP in cell culture media following incubation of RKO cells with increasing amounts of nano- (nZnO, ▼) and microsized (mZnO, ▲) ZnO for 24 h.

the 10 ($p < 0.01$) and the 30 μg/cm^2 ($p < 0.001$) concentrations. Cell-free control experiments showed that possible ZnO particulate interactions with the test reagent did not alter the absorbance as compared to blank controls.

We measured the amount of Zn^{2+} in the cell culture media following 24 h incubations of RKO cells with increasing concentrations of the nZnO and mZnO. We observed a dependence on the amount of the solid phase that was different between the two particle sizes, suggesting that the observed ZnO concentration in the media was controlled by reaction kinetics or mass transfer under the conditions of our cell culture experiments (Figure 4).

We compared three protocols to evaluate whether ZnO cytotoxicity requires direct particle-to-cell contact: (1) We evaluated both nZnO and mZnO that were separated from the cell-containing culture media by inserting the particulate matter inside a dialysis cassette with a 10 kDa molecular mass cut off; (2) we plated cells on top of a Transwell insert with 0.4 μm pores, and the ZnO particulate matter was placed into the lower compartment of the well; and (3) we exposed the cells directly to ZnO particulate matter that was added to the media above the cells. In all cases, cell exposures were conducted at particle suspension concentrations equivalent to 30 μg/cm^2 of the cell growth surface for a conventional in vitro particle exposure. This was a concentration that was clearly cytotoxic for the nZnO and mZnO (Figure 3). Both the sizes of the agglomerates measured by DLS and the observation of the wells by light microscopy confirm that the nanoparticles were able to settle to the bottom of the culture well within the time scale of the cell exposures. The total ZnO content in each cell culture well was comparable between the different conditions, but it differed in availability to the cells. We measured Zn content by ICP in the supernatant media collected from biological triplicates. The amount of liberated Zn in cell-free media controls and cassette samples was minimal due to the accumulation of the ZnO agglomerates in the bottom of the well or in the central cavity of the dialysis cassette, respectively, but the Zn concentration was considerably elevated in the Transwell and direct contact samples, which contained viable cells (Figure 5A). At the same particle concentration, 30 μg/cm^2, and time, 24 h, the amount of Zn in the cell-free media was significantly less than for incubation with RKO cells (Figure 4). The effect of RKO cells and the effects of the different cell culture well configurations on the concentration of Zn in the cell culture media suggest that the transfer of Zn^{2+} from the solid to the aqueous phase is

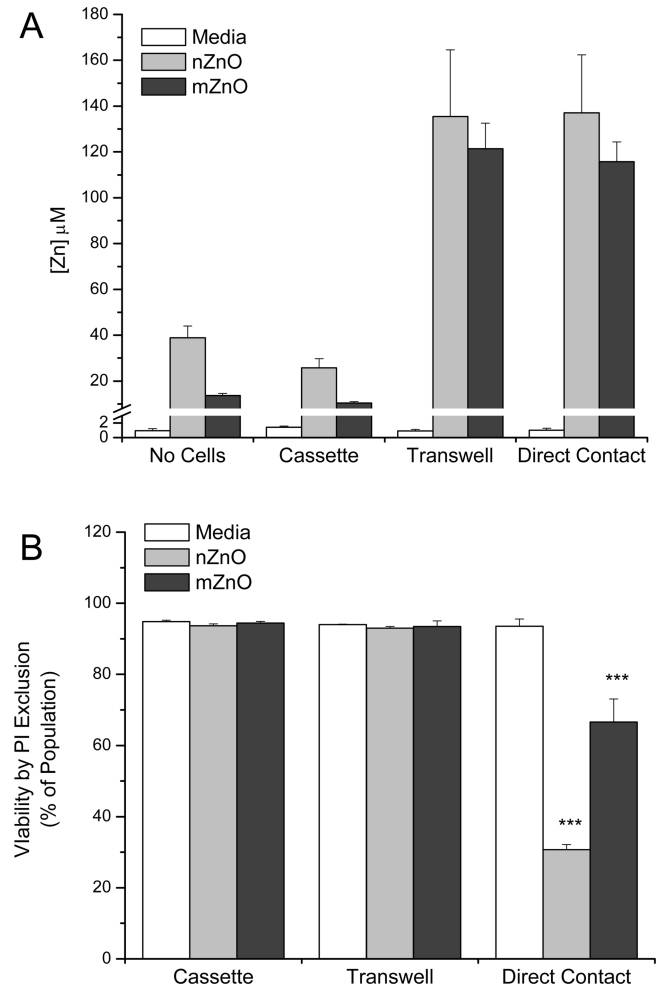

Figure 5. ZnO contact-dependent cell death in RKO cells. (A) Soluble Zn levels measured by ICP spectrometry for nZnO (30 μg/cm^2) diluted in tissue culture media (No Cells), in media injected into a Slide-A-Lyzer cassette with a 10 kDa molecular mass cutoff (Cassette), in the lower chamber of a cell culture transwell system with the RKO cells in the insert (Transwell), and in direct contact with the RKO cells (Direct Contact). (B) Cellular viability as measured by PI exclusion for the three conditions containing cells: Cassette, Transwell, and Direct Contact, showing only direct contact influenced cell viability (***$p <$ 0.001).

mediated by substances secreted by the cells. The 10 kDa cutoff membrane appears to prevent the solublized Zn from diffusing into the media, which would suggest that the aqueous phase Zn is in a high molecular mass complex. Because the cells and particles were physically separated in the Transwells, the observed Zn dissolution results are not consistent with a mechanism involving particle uptake, intracellular dissolution, and subsequent release of dissolved Zn^{2+} back into the media.

We evaluated the viability of the cells in these experiments using PI exclusion, and only those cells in direct contact with the ZnO particulate matter displayed decreased viability (Figure 5B) even though the transwells contained similar levels of Zn in the media. Therefore, in RKO cells, direct particle−cell contact was required for decreased cellular viability, and cytotoxicity was independent of the liberated Zn levels. Similar to the viability analysis, the nZnO was significantly more toxic ($p < 0.01$) than the mZnO.

To elucidate the mechanism of ZnO-dependent cytotoxicity, we examined RKO cells after 10 μg/cm^2 ZnO treatment for 24 h. This evaluated early stages of cell damage rather than the final loss of membrane integrity, indicated by PI staining, observed at 30 μg/cm^2 (Figure 5B). First, the mechanism of ZnO

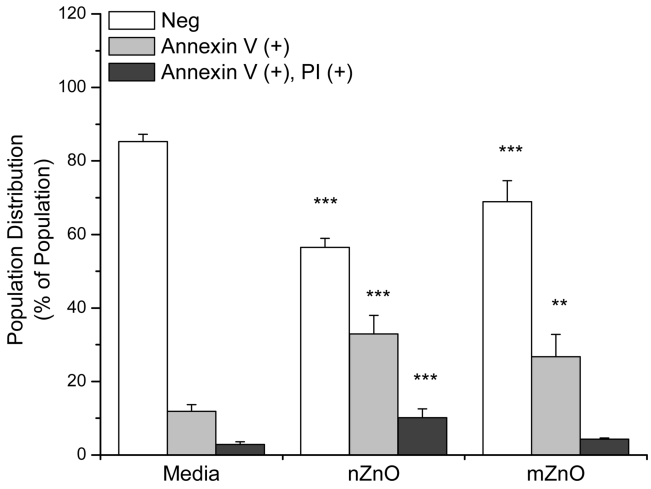

Figure 6. Annexin V and PI staining of RKO cells treated with nZnO particulate matter. Treated RKO cells demonstrate increased Annexin V positive/PI negative [Annexin V (+); $^{**}p < 0.01$; $^{***}p < 0.001$] labeling with only modest increases in Annexin V positive/PI positive [Annexin V (+), PI (+); $^{***}p < 0.001$] labeling in the nZnO treatment. The percentage of the cells was recorded where the cells that were not stained (Neg) represent viable cells, Annexin V positive represents early apoptotic cells, and Annexin V plus PI double positive represents late apoptotic or necrotic cells. The percentage of Annexin V positive cells significantly changes with nZnO treatment.

particulate-mediated cell death was evaluated with Annexin V binding and PI exclusion to detect early stage apoptosis. Early apoptotic cells display phosphatidylserine on the outer surface of the cell membrane where Annexin V can bind when the membrane is still intact. Necrotic cells and late apoptotic cells have disrupted membranes that are permeable to Annexin V and PI. Three cell populations were measured as follows: (1) the fluorescent negative population representing viable cells, (2) Annexin V positive, PI negative population representing early apoptotic cells, and (3) Annexin V positive plus PI positive population representing late apoptotic or necrotic cells. Both nano- and microsized ZnO treatments increased the amount of Annexin V binding (Figure 6), and ≥90% of the cells were PI negative suggesting activation of apoptosis pathways.

To further elucidate cell damage mechanisms, we evaluated mitochondrial responses, because elevated intracellular Zn^{2+} has been correlated with mitochondrial dysfunction (*27*). First, we used JC-1 to measure the mitochondrial membrane potential. JC-1 is a mitochondrion-selective compound that displays differential fluorescence based on the potential across the mitochondrial membrane, and we observed significant disruption of mitochondrial potential in cells treated with 10 μg/cm^2 of nZnO and mZnO (Figure 7A). Next, we used the mitochondrion-selective dye MitoSOX Red to measure the production of superoxide, and we found that ZnO treatments also increased the production of superoxide (Figure 7B). For both the JC-1 and the MitoSOX assay, the nZnO treatment was significantly ($p < 0.01$) more disruptive to mitochondrial function than the mZnO treatment. Because we observed soluble Zn at a concentration of ~100 μM with cell treatment at 10 μg/cm^2 (Figure 4), we performed the JC-1 and MitoSOX assay with RKO cells exposed to 100 μM $ZnCl_2$ to address the likelihood that soluble Zn^{2+} might alter mitochondrial function. No changes in were observed in either assay with $ZnCl_2$ treatment. Therefore, robust hallmarks of apoptosis, including Annexin V staining, loss of mitochondrial potential, and increased generation of superoxide, were observed when cells were treated with ZnO particulate matter but not a soluble Zn salt.

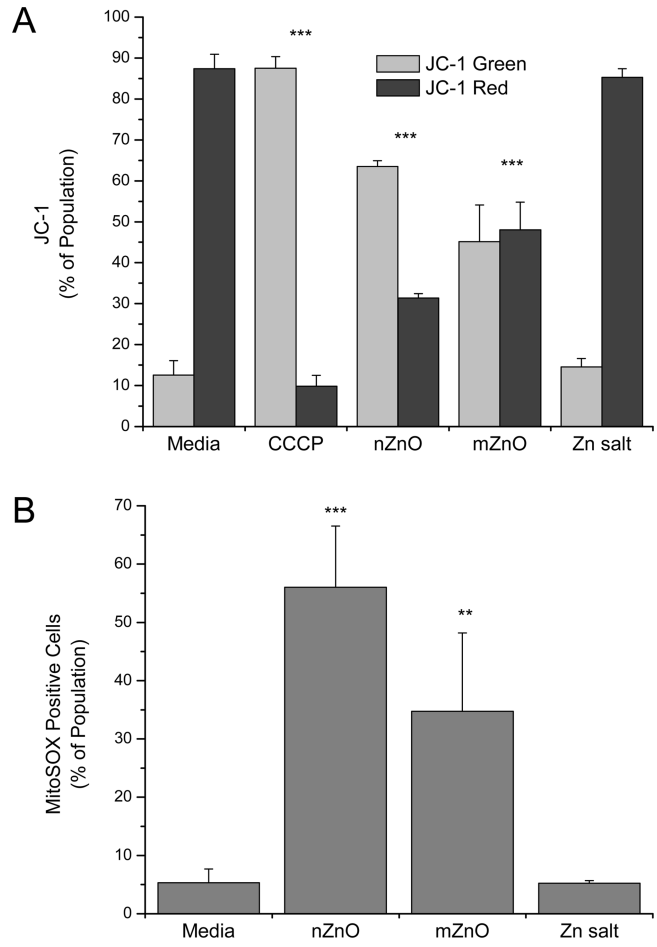

Figure 7. Mitochondrial dysfunction follows incubation with ZnO but not $ZnCl_2$. (A) ZnO at 10 μg/cm^2 results in disruption of mitochondria mitochondrial potential (nZnO and mZnO), but 100 μM $ZnCl_2$ (Zn salt) does not disrupt the mitochondrial potential. JC-1 fluoresces green when the mitochondrial potential has been depolarized and forms aggregates that fluoresce red when the mitochondrion is normally polarized. Carbonyl cyanide 3-chlorophenylhydrazone (CCCP) was used at 25 μM to disrupt the mitochondrial membrane potential as a positive control. CCCP, nanoZnO, and microZnO were significantly different ($p < 0.001$) than the media and $ZnCl_2$ samples. (B) MitoSOX Red staining displays low levels of superoxide production in untreated cells (Media) and significantly increased superoxide production ($^{***}p < 0.001$; $^{**}p < 0.01$) following ZnO treatments but no differences from control in 100 μM $ZnCl_2$ (Zn salt) treated RKO cells. The cells were directly evaluated by flow cytometry, and the percentage of the population that displayed fluorescence was quantified.

Discussion

A key question in the toxicology of novel nanomaterials is the effect of high specific surface area solids as compared to the effects of soluble moieties released from the particles. When the solid ZnO was physically separated from the RKO cells, there was minimal cytotoxicity even though the Zn concentration in the aqueous medium was similar to the experiments showing cytotoxicity when the particles were in direct contact with the cells. The effect of particle size and shape on toxicity is another current question, and many studies have suggested that dose expressed as surface area is the most relevant quantity. Correlation of cytotoxicity with size has been reported with macrophages exposed to silica particles (*28*) and with bacteria and osteoblast cells exposed to ZnO (*12*). We saw statistically significant, but relatively modest, differences between the nZnO and the mZnO. These differences between studies may be due to the cell types used, but other studies have also not shown distinctive particulate size effects related to

toxicity (*8*). On the U.S. Standard Sieve Series, the 325 mesh screen corresponds to 44 μm openings. However, the electron microscopy and gas adsorption surface measurements suggest that the nominally −325 mesh powder actually contained submicrometer particles. The ratio of specific surface area between the nZnO and the mZnO was only about 7-fold, which is much smaller than the 5000-fold ratio of the nominal nanoparticle size to the nominal screen size. The common industrial process for producing ZnO involves vaporization of zinc metal followed by rapid oxidation. Agglomerated powders consisting of fused aggregates of smaller particles are commonly produced both by synthesis processes that involve metal vaporization followed by gas-to-solid conversion (*29*) and as an incidental byproduct of combustion systems (*30*). Particle size and fractal structure affect mass transfer, while agglomerate size affects the rate of sedimentation in cell culture wells. The biological implications of aggregation (physical fusing) of the initially formed particles versus agglomeration (attachment only by weak surface forces) on the biological effects of particles are an area of active research (*31*).

It is unclear whether nanoparticulate dietary metal oxides, including ZnO, have chronic effects on the colon. Ingestion of large amounts of ZnO has been reported to cause gastroduodenal corrosive injury in humans without systemic toxicity (*22*). Inhaled ZnO can cause pulmonary toxicity (*16*−*20*) but is generally considered to have minimal toxicity in other organs (*32*). Increased consumption of fine and ultrafine particulate matter is hypothesized to exacerbate inflammatory bowel disease (*33*−*36*) possibly due to transport of substances adsorbed on the solid surface (*4*). A study of patients with Crohn's disease showed that a low microparticle diet was beneficial (*35*), but a follow-up study did not confirm the original findings (*37*). In rodent studies, particles smaller than 100 nm were taken up by the rat intestinal mucosa and enter systemic circulation (*38*), plus inflamed colon cells internalize nanoparticles at a greater rate than normal colon cells (*39*). In humans, observations of tissue biopsies from patients with Crohn's disease or cancer contain nanoparticles of exogenous origin (*40*).

The concentrations used in this study are high based on treated cell culture well surface area but not implausible on a suspended volume basis. The maximum in vitro cell treatment was approximately 100 μg/mL. Assuming 1.5−2 L as the volume entering the colon per day (*41*), this concentration could be reached by ingesting 2 g of a lotion containing 10% ZnO. However, unlike TiO_2 and SiO_2, which are also used in cosmetics and sunscreens, ZnO nanoparticles are likely to dissolve in the low pH environment of the stomach (*22*). Because we have demonstrated that ZnO particulate must come into contact with cells to initiate cytotoxic effects, it may be that particulate ZnO has a low potential for toxicity by incidental consumption. We are aware of no recent animal or human studies of nanosized ZnO taken orally at doses much higher than nutritional levels.

In this study, we measured the liberated Zn from ZnO nano- and microsized particulate matter and determined that the toxicity in RKO cells is dependent on cell contact with the particulate matter rather than just exposure to high levels of soluble Zn and further showed that the cytotoxicity involves apoptosis pathways. ZnO in consumer products, such as sunscreens, can lead to ingestion exposure, especially in children. Evidence of cell death and mitochondrial changes in response to ZnO particle contact supports further study in animal models. These colon cell studies of particles sold as novel nanomaterials and as conventional screen-sized powders showed a limited, but observable, size-dependent difference in ZnO particle potency but similar mechanisms of toxicity. It would be of interest in further work to determine if cell uptake, or simply cell contact, is required for cytotoxicity.

Acknowledgment. This work was funded by U.S. EPA-Science to Achieve Results (STAR) program, and Grants RD83333601 (P.J.M.) and RD8317230 (J.M.V.). We also acknowledge the use of core facilities supported by P30 CA042014 awarded to Huntsman Cancer Institute and Zetasizer instrument and ICP spectrometer access provided by H. Ghandehari and D. Winge, respectively.

References

(1) Oberdorster, G., Oberdorster, E., and Oberdorster, J. (2005) Nanotoxicology: An emerging discipline evolving from studies of ultrafine particles. *Environ. Health Perspect. 113*, 823–839.
(2) Warheit, D. B., Sayes, C. M., Reed, K. L., and Swain, K. A. (2008) Health effects related to nanoparticle exposures: Environmental, health and safety considerations for assessing hazards and risks. *Pharmacol. Ther. 120*, 35–42.
(3) Faunce, T. A. (2009) Safety of nanoparticles in sunscreens. *Med. J. Aust. 190*, 463.
(4) Schneider, J. C. (2007) Can microparticles contribute to inflammatory bowel disease: Innocuous or inflammatory? *Exp. Biol. Med. (Maywood) 232*, 1–2.
(5) Chau, C.-F., Wu, S.-H., and Yen, G.-C. (2007) The development of regulations for food nanotechnology. *Trends Food Sci. Technol. 18*, 269–280.
(6) Miller, G., Archer, L., Pica, E., Bell, D., Senjen, R., and Kimbrell, G. (2006) Nanomaterials sunscreens and cosmetics: Small ingredients big risks, http://nano.foe.org.au, Friends of the Earth.
(7) Veranth, J. M., Kaser, E. G., Veranth, M. M., Koch, M., and Yost, G. S. (2007) Cytokine responses of human lung cells (BEAS-2B) treated with micron-sized and nanoparticles of metal oxides compared to soil dusts. *Part. Fibre Toxicol. 4*, 2.
(8) Adams, L. K., Lyon, D. Y., and Alvarez, P. J. (2006) Comparative eco-toxicity of nanoscale TiO2, SiO2, and ZnO water suspensions. *Water Res. 40*, 3527–3532.
(9) Franklin, N. M., Rogers, N. J., Apte, S. C., Batley, G. E., Gadd, G. E., and Casey, P. S. (2007) Comparative toxicity of nanoparticulate ZnO, bulk ZnO, and ZnCl2 to a freshwater microalga (*Pseudokirchneriella subcapitata*): The importance of particle solubility. *Environ. Sci. Technol. 41*, 8484–8490.
(10) Gojova, A., Guo, B., Kota, R. S., Rutledge, J. C., Kennedy, I. M., and Barakat, A. I. (2007) Induction of inflammation in vascular endothelial cells by metal oxide nanoparticles: Effect of particle composition. *Environ. Health Perspect. 115*, 403–409.
(11) Heinlaan, M., Ivask, A., Blinova, I., Dubourguier, H. C., and Kahru, A. (2008) Toxicity of nanosized and bulk ZnO, CuO and TiO2 to bacteria Vibrio fischeri and crustaceans *Daphnia magna* and *Thamnocephalus platyurus*. *Chemosphere 71*, 1308–1316.
(12) Nair, S., Sasidharan, A., Divya Rani, V. V., Menon, D., Nair, S., Manzoor, K., and Raina, S. (2009) Role of size scale of ZnO nanoparticles and microparticles on toxicity toward bacteria and osteoblast cancer cells. *J. Mater. Sci. Mater. Med. 20*, S235–S241.
(13) Reddy, K. M., Feris, K., Bell, J., Wingett, D. G., Hanley, C., and Punnoose, A. (2007) Selective toxicity of zinc oxide nanoparticles to prokaryotic and eukaryotic systems. *Appl. Phys. Lett. 90*, 2139021–2139023.
(14) Sayes, C. M., Reed, K. L., and Warheit, D. B. (2007) Assessing toxicity of fine and nanoparticles: Comparing in vitro measurements to in vivo pulmonary toxicity profiles. *Toxicol. Sci. 97*, 163–180.
(15) Zhu, X., Zhu, L., Duan, Z., Qi, R., Li, Y., and Lang, Y. (2008) Comparative toxicity of several metal oxide nanoparticle aqueous suspensions to Zebrafish (*Danio rerio*) early developmental stage. *J. Environ. Sci. Health, Part A: Toxic/Hazard. Subst. Environ. Eng. 43*, 278–284.
(16) Lindahl, M., Leanderson, P., and Tagesson, C. (1998) Novel aspect on metal fume fever: Zinc stimulates oxygen radical formation in human neutrophils. *Hum. Exp. Toxicol. 17*, 105–110.
(17) Gordon, T., Chen, L. C., Fine, J. M., Schlesinger, R. B., Su, W. Y., Kimmel, T. A., and Amdur, M. O. (1992) Pulmonary effects of inhaled zinc oxide in human subjects, guinea pigs, rats, and rabbits. *Am. Ind. Hyg. Assoc. J. 53*, 503–509.
(18) Lam, H. F., Chen, L. C., Ainsworth, D., Peoples, S., and Amdur, M. O. (1988) Pulmonary function of guinea pigs exposed to freshly generated

ultrafine zinc oxide with and without spike concentrations. *Am. Ind. Hyg. Assoc. J. 49*, 333–341.
(19) Conner, M. W., Flood, W. H., Rogers, A. E., and Amdur, M. O. (1988) Lung injury in guinea pigs caused by multiple exposures to ultrafine zinc oxide: Changes in pulmonary lavage fluid. *J. Toxicol. Environ. Health 25*, 57–69.
(20) Lam, H. F., Conner, M. W., Rogers, A. E., Fitzgerald, S., and Amdur, M. O. (1985) Functional and morphologic changes in the lungs of guinea pigs exposed to freshly generated ultrafine zinc oxide. *Toxicol. Appl. Pharmacol. 78*, 29–38.
(21) Barceloux, D. G. (1999) Zinc. *J. Toxicol. Clin. Toxicol. 37*, 279–292.
(22) Liu, C. H., Lee, C. T., Tsai, F. C., Hsu, S. J., and Yang, P. M. (2006) Gastroduodenal corrosive injury after oral zinc oxide. *Ann. Emerg. Med. 47*, 296.
(23) Wesselkamper, S. C., Chen, L. C., and Gordon, T. (2001) Development of pulmonary tolerance in mice exposed to zinc oxide fumes. *Toxicol. Sci. 60*, 144–151.
(24) Berridge, M. V., Herst, P. M., and Tan, A. S. (2005) Tetrazolium dyes as tools in cell biology: New insights into their cellular reduction. *Biotechnol. Annu. Rev. 11*, 127–152.
(25) Salvioli, S., Ardizzoni, A., Franceschi, C., and Cossarizza, A. (1997) JC-1, but not DiOC6(3) or rhodamine 123, is a reliable fluorescent probe to assess delta psi changes in intact cells: Implications for studies on mitochondrial functionality during apoptosis. *FEBS Lett. 411*, 77–82.
(26) Park, M. V., Annema, W., Salvati, A., Lesniak, A., Elsaesser, A., Barnes, C., McKerr, G., Howard, C. V., Lynch, I., Dawson, K. A., Piersma, A. H., and de Jong, W. H. (2009) In vitro developmental toxicity test detects inhibition of stem cell differentiation by silica nanoparticles. *Toxicol. Appl. Pharmacol. 240*, 108–116.
(27) Gazaryan, I. G., Krasinskaya, I. P., Kristal, B. S., and Brown, A. M. (2007) Zinc irreversibly damages major enzymes of energy production and antioxidant defense prior to mitochondrial permeability transition. *J. Biol. Chem. 282*, 24373–24380.
(28) Waters, K. M., Masiello, L. M., Zangar, R. C., Tarasevich, B. J., Karin, N. J., Quesenberry, R. D., Bandyopadhyay, S., Teeguarden, J. G., Pounds, J. G., and Thrall, B. D. (2009) Macrophage responses to silica nanoparticles are highly conserved across particle sizes. *Toxicol. Sci. 107*, 553–569.
(29) Flagan, R. C. (1994) Dynamics of Pyrogenous Fumes. *Fuel Process. Technol. 39*, 319–336.
(30) Lighty, J. S., Veranth, J. M., and Sarofim, A. F. (2000) Combustion aerosols: Factors governing their size and composition and implications to human health. *J. Air Waste Manage. Assoc. 50*, 1565–1618; discussion 1619−1522.
(31) Murdock, R. C., Braydich-Stolle, L., Schrand, A. M., Schlager, J. J., and Hussain, S. M. (2008) Characterization of nanomaterial dispersion in solution prior to in vitro exposure using dynamic light scattering technique. *Toxicol. Sci. 101*, 239–253.
(32) Sax, N. I., and Lewis, R. J. (1989) *Dangerous Properties of Industrial Materials*, 7th ed., Van Nostrand Reinhold, New York.
(33) Lomer, M. C., Hutchinson, C., Volkert, S., Greenfield, S. M., Catterall, A., Thompson, R. P., and Powell, J. J. (2004) Dietary sources of inorganic microparticles and their intake in healthy subjects and patients with Crohn's disease. *Br. J. Nutr. 92*, 947–955.
(34) Lomer, M. C., Thompson, R. P., and Powell, J. J. (2002) Fine and ultrafine particles of the diet: influence on the mucosal immune response and association with Crohn's disease. *Proc. Nutr. Soc. 61*, 123–130.
(35) Lomer, M. C., Harvey, R. S., Evans, S. M., Thompson, R. P., and Powell, J. J. (2001) Efficacy and tolerability of a low microparticle diet in a double blind, randomized, pilot study in Crohn's disease. *Eur. J. Gastroenterol. Hepatol. 13*, 101–106.
(36) Powell, J. J., Harvey, R. S., Ashwood, P., Wolstencroft, R., Gershwin, M. E., and Thompson, R. P. (2000) Immune potentiation of ultrafine dietary particles in normal subjects and patients with inflammatory bowel disease. *J. Autoimmun. 14*, 99–105.
(37) Lomer, M. C., Grainger, S. L., Ede, R., Catterall, A. P., Greenfield, S. M., Cowan, R. E., Vicary, F. R., Jenkins, A. P., Fidler, H., Harvey, R. S., Ellis, R., McNair, A., Ainley, C. C., Thompson, R. P., and Powell, J. J. (2005) Lack of efficacy of a reduced microparticle diet in a multi-centred trial of patients with active Crohn's disease. *Eur. J. Gastroenterol. Hepatol. 17*, 377–384.
(38) Jani, P., Halbert, G. W., Langridge, J., and Florence, A. T. (1990) Nanoparticle uptake by the rat gastrointestinal mucosa: Quantitation and particle size dependency. *J. Pharm. Pharmacol. 42*, 821–826.
(39) Lamprecht, A., Yamamoto, H., Takeuchi, H., and Kawashima, Y. (2005) Nanoparticles enhance therapeutic efficiency by selectively increased local drug dose in experimental colitis in rats. *J. Pharmacol. Exp. Ther. 315*, 196–202.
(40) Gatti, A. M. (2004) Biocompatibility of micro- and nano-particles in the colon. Part II. *Biomaterials 25*, 385–392.
(41) Sandle, G. I. (2007) Salt and water absorption in the human colon: A modern appraisal. *Gut 43*, 294–299.

TX900203V